

## Novel Nanofibrous Dy<sub>2</sub>Ce<sub>2</sub>O<sub>7</sub> as an Electrocatalyst for Methanol Oxidation

Aijuan Zhao<sup>1</sup>, Haijie Sun<sup>1\*</sup>, Lingxia Chen<sup>1</sup>, Yufang Huang<sup>1</sup>, Mubing<sup>1</sup>, Xingjie Lu<sup>2\*</sup>, Hairong Gao<sup>1</sup>, Yaping Wang<sup>1</sup>, Xiuli Chen<sup>1</sup>

<sup>1</sup> Institute of Environmental and Catalytic Engineering, College of chemistry and chemical engineering, Zhengzhou Normal University, Zhengzhou 450044, Henan, China

<sup>2</sup> Henan Institute of Metrology, Zhengzhou 450000, Henan, China

\*E-mail: [sunhaijie406@zznu.edu.cn](mailto:sunhaijie406@zznu.edu.cn), [xingjieluzznu@163.com](mailto:xingjieluzznu@163.com)

Received: 28 March 2019/ Accepted: 21 May 2019 / Published: 30 June 2019

---

The present paper has utilized nanoparticles of fibrous Dy<sub>2</sub>Ce<sub>2</sub>O<sub>7</sub>. The catalytic strength of fibrous Dy<sub>2</sub>Ce<sub>2</sub>O<sub>7</sub> was used as an electrocatalyst in the case of methanol oxidation reaction. The fibrous Dy<sub>2</sub>Ce<sub>2</sub>O<sub>7</sub> NPs are completely investigated by taking advantages of AFM, XRD, EDS, BET, TEM, FESEM and FT-IR analyses. The fibrous Dy<sub>2</sub>Ce<sub>2</sub>O<sub>7</sub> indicated high stability for reaction without considerable loss of some property like activity.

---

**Keywords:** Electrocatalyst, Nano catalyst, Dy<sub>2</sub>Ce<sub>2</sub>O<sub>7</sub>, Green chemistry, Nanoparticle

### 1. INTRODUCTION

Bimetallic nanoparticles are promising materials due to their porous, large surface zones, abundant active sites, and open structures subjected on the branched surfaces [1-10]. Assessment of Re<sub>2</sub>Ce<sub>2</sub>O<sub>7</sub> as a rare earth cerate are gaining importance because of its wide applications in diverse fields [11-18]. Diverse methods have been presented to synthesis the rare earth cerate [19-22]. This technique is not cost impressive and not eco-friendly viable because of the usage of harmful chemical material, or complex cases during preparation. Therefore, there is main need to drop the harmful chemical materials as well as to present clean and also effective technique to fabricate the nano-scale rare earth cerate.

Direct methanol fuel cells (DMFC) are regarded as the most promising power source in the future and can be applied to mobile devices and portable devices [23-25]. Concerning the catalysts for DMFC, metal based materials are widely used. However, there are still drawbacks for conventional catalysts, such as low efficiency, high cost, poor stability and durability. These drawbacks limit the

employment of DMFC to a large extent [26-33]. Thus, increase the activity and stability of Pt catalysts as well as reducing the cost of Pt catalysts will be more practical for the development of DMFC.

Due to high-index forms have a high density of low-coordinated compared to other similar materials step atoms by high reactivity. In the present paper, a new fibrous  $\text{Dy}_2\text{Ce}_2\text{O}_7$  nanostructures with having noteworthy properties are produced and selected as electrocatalyst for the oxidation reaction of methanol in an aqueous medium. The system of Microemulsion caused to form a novel morphology of mesoporous  $\text{Dy}_2\text{Ce}_2\text{O}_7$  with having dendrimeric fibers developed outward producing a high surface area as well as high availability of the reactant to the functional compounds. The production of fibrous  $\text{Dy}_2\text{Ce}_2\text{O}_7$  nanoparticles has been realized by reduction of a ceric ammonium nitrate as well as dysprosium nitrate on the templates of sacrificial polymeric micelle.  $\text{Dy}_2\text{Ce}_2\text{O}_7$  nanostructure is unique with this kind of fibrous morphology.

## 2. EXPERIMENTAL

High purity chemicals were procured from Fluka and Merck. Electrothermal 9100 apparatus were utilized for the determination of uncorrected melting points in open capillaries. VERTEC 70 spectrometer (Bruker) in transmission mode were used for the determination of FTIR spectra. Samples were pulverized and pelletized with spectroscopic grade KBr. Determination of size and structure of nano particles were done via transmission electron microscope (TEM) (Phillips CM10) operated at 100 kV. The crystallographic structures of nano particles are characteristics by utilizing powder X-ray diffraction (Bruker D8 Advance model) with Cu  $\text{K}\alpha$  radiation. Thermal gravimetry analysis (TGA) (NETZSCH STA449F3) is used with a heating rate of  $10^\circ\text{C}/\text{min}$  (under nitrogen atmosphere). NMR spectra of  $^1\text{H}$  and  $^{13}\text{C}$  were determined with BRUKER DRX-300 AVANCE spectrometer and BRUKER DRX-400 AVANCE spectrometer. The NMR spectra recorded for both elements were at 300.13 and 75.46 MHz; 400.22 and 100.63 MHz, respectively. Heraeus CHN-O-Rapid analyzer were used to perform elemental analyses for carbon, hydrogen and nitrogen. Thin layer chromatography (TLC) done on silica gel polygramSILG/UV 254 plates were used for the determination of product purity and monitoring of reaction. Shimadzu GCMS-QP5050 Mass Spectrometer were used to map the mass spectra.

### 2.2. General procedure for the preparation of fibrous $\text{Dy}_2\text{Ce}_2\text{O}_7$ NPs

1.1 ml of aqueous 45 mM ammonium nitrate as well as 45 mM dysprosium nitrate is dissolved in a cyclohexane solution (0.3 L) and 1-pentanol (0.015 L). A solution of the stirred cetylpyridinium bromide (CPB 1 g) and 0.001 l of aqueous 0.1 M ascorbic acid is also added. The out coming mixture is stirred during 45 min under the temperature of  $25^\circ\text{C}$  and also placed in a reactor of teflon-sealed hydrothermal and heated under the temperature of  $100^\circ\text{C}$  for 5 hours. The fibrous  $\text{Dy}_2\text{Ce}_2\text{O}_7$  NPs are after wards isolated using centrifugation, washed by deionized water as well as acetone and dried under heating of a drying oven.

### 2.3. Preparation of working electrode

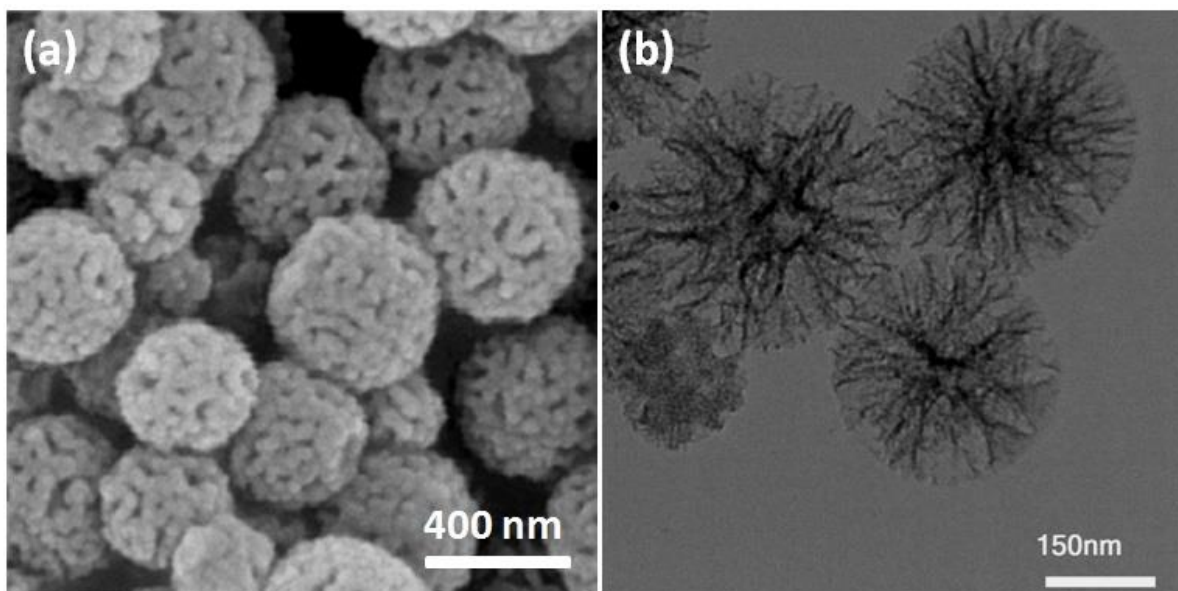
A glassy carbon electrode (GCE) with having a diameter around 3 mm and active surface zone of  $0.071 \text{ cm}^2$  is burnished by slurry of alumina powder and then cleaned by deionized water. A certain amount of catalyst was evenly scattered in around  $1000 \mu\text{L}$  deionized water by ultrasonication. After that,  $8 \mu\text{L}$  of the catalyst suspension was dropped onto the GCE. After the catalyst suspension was dried,  $6 \mu\text{L}$  of 0.5% Nafion released onto the GCE. The GCE is dried in air before use. The mass loading of Pt on GCE is about  $8 \mu\text{g}$  for whole considered catalysts.

### 2.4. Electrochemical tests

The electrochemical performances are tested by using a three-electrode cell on a CHI-660D model electrochemical workstation at room temperature. The base electrode was a saturated calomel electrode (SCE). Then the auxiliary electrode was a platinum electrode ( $2\text{cm} \times 2\text{cm}$ ). In the cyclic voltammetry (CV) tests, the scanning rate was  $50 \text{ mV/s}$ , and the potential window was  $-0.2 \sim 1.0 \text{ V}$ . The electrolytes were  $\text{N}_2$  saturated  $0.5 \text{ M H}_2\text{SO}_4$  solution or  $\text{N}_2$  saturated  $0.5 \text{ M H}_2\text{SO}_4 + 0.5 \text{ M CH}_3\text{OH}$  solution. The data were recorded after the figure tend stable. The chronoamperometry experiments were performed at  $0.6 \text{ V}$  for  $3600 \text{ s}$  in  $0.5 \text{ M H}_2\text{SO}_4 + 0.5 \text{ M CH}_3\text{OH}$ .

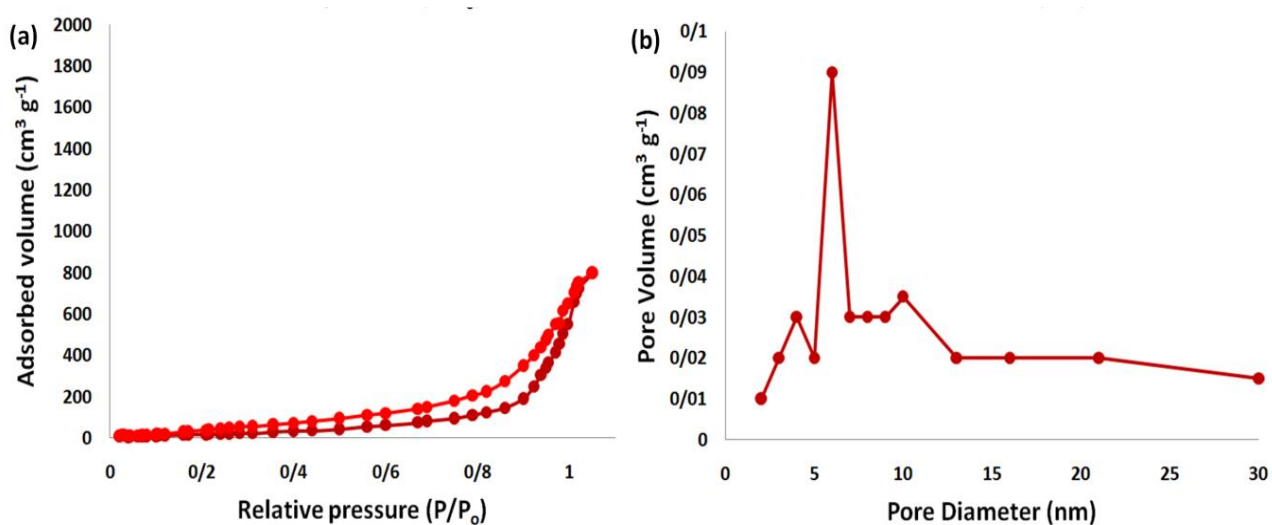
## 3. RESULTS AND DISCUSSION

The dendritic fibrous nano  $\text{Dy}_2\text{Ce}_2\text{O}_7$  was produced using a simple approach. The produced fibrous nano  $\text{Dy}_2\text{Ce}_2\text{O}_7$  was then determined using various methods like AFM, XRD, EDS, BET, TEM, FESEM, and FT-IR. The morphology as well as structure of the dendritic fibrous nano  $\text{Dy}_2\text{Ce}_2\text{O}_7$  are well marked using TEM and FESEM analysis. SEM image of dendritic  $\text{Dy}_2\text{Ce}_2\text{O}_7$  nanoparticles indicates dandelion-like structure with diameters around  $\sim 300 \text{ nm}$  and also a wrinkled radial structure (as can be seen in Figure 1a). In addition, this fiber with thicknesses of  $\sim 8.5 \text{ nm}$  enhances from the center of the considered spheres and are increase in all radial dimensions (can be seen in Figure 1b). Moreover, the excessive increasing of the wrinkled radial construction makes cone-shaped open pores. The obtained image of FESEM and TEM illustrates, which the whole sphere is completely solid and consisted of fibers. Also, this structure of open hierarchical channel as well as considered fibers are lightly for the mass transfer in the case of reactants and enhance the availability of active sites.



**Figure 1.** FESEM images of  $Dy_2Ce_2O_7$  NPs (a); TEM images of  $Dy_2Ce_2O_7$  NPs (b).

The analysis of nitrogen physisorption indicated that the BET specific surface area of the dendritic fibrous nano  $Dy_2Ce_2O_7$  were around  $209 \text{ m}^2/\text{g}$ . As can be observed in Figure 2, the nitrogen adsorption-desorption isotherms of the dendritic fibrous nano  $Dy_2Ce_2O_7$  based catalysts. The dendritic fibrous nano  $Dy_2Ce_2O_7$  indicated a kind IV isotherm, by a H1-type hysteresis loop, proposing the attendance of mesopores. The corresponding pore size dispensation predicted from the desorption series of the nitrogen isotherm using the BJH procedure displayed a narrowpore size distribution peaked at about 6 nm (as can be seen Table 1).

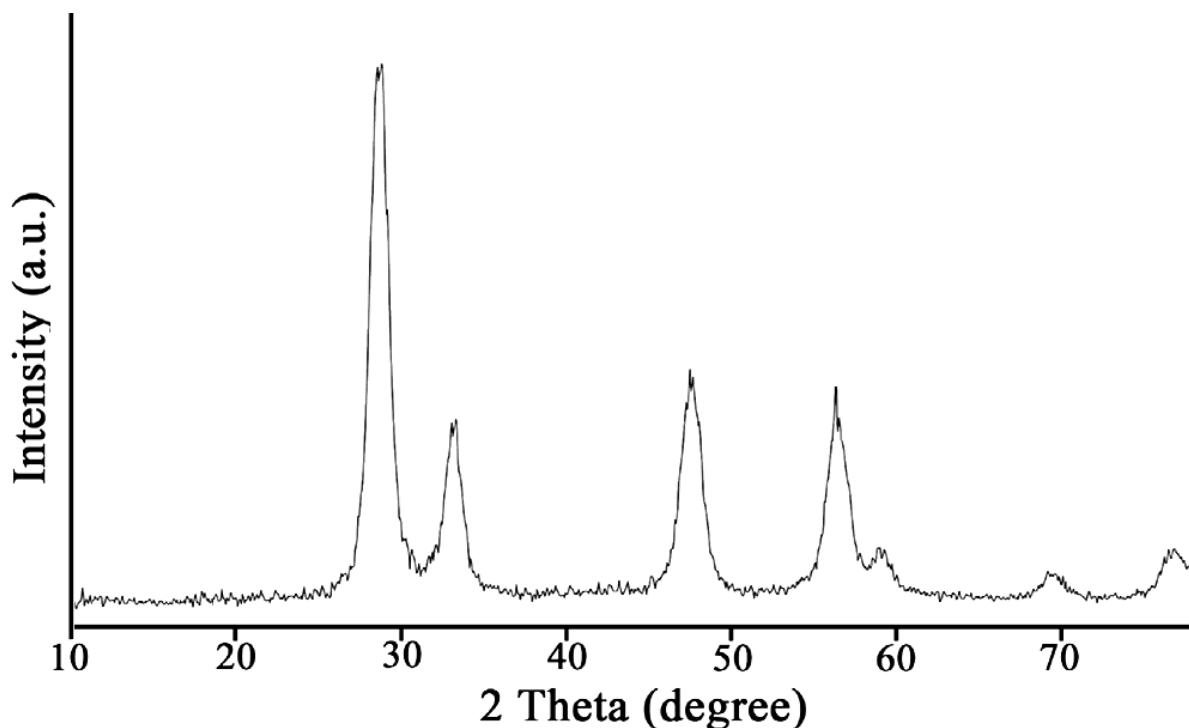


**Figure 2.** adsorption-desorption isotherms of the  $Dy_2Ce_2O_7$  NPs (a); BJH pore size distributions of the  $Dy_2Ce_2O_7$  NPs (b).

**Table1.** Structural parameters of Dy<sub>2</sub>Ce<sub>2</sub>O<sub>7</sub> NPs.

Catalysts	S <sub>BET</sub> (m <sup>2</sup> g <sup>-1</sup> )	V <sub>a</sub> (cm <sup>3</sup> g <sup>-1</sup> )	D <sub>BJH</sub> (nm)
Fibrous nano Dy <sub>2</sub> Ce <sub>2</sub> O <sub>7</sub>	209	1.4	6

The analysis of XRD that is highly useful method to determine crystalline structure as well as average crystallite size, is used to test the as-obtained nanostructured Dy<sub>2</sub>Ce<sub>2</sub>O<sub>7</sub>. Total the diffraction peaks showed in Figure 3 are properly matched with pure fluorite Dy<sub>2</sub>Ce<sub>2</sub>O<sub>7</sub>. As seen no impurities existed in this schema. The surface roughness of Dy<sub>2</sub>Ce<sub>2</sub>O<sub>7</sub> NPs in its fibrous shape is too characterized using atomic force microscopy (AFM) as well as the images of topographic that are shown in Figure 4. As seen, the more height region determined using the brighter yellowish white color enhanced by reducing T/W, proposing the roughness increase in the surface of catalyst. Figure 5 demonstrated which FT-IR spectrum which analyzed to obtain more details concerning surface of the created nanostructured Dy<sub>2</sub>Ce<sub>2</sub>O<sub>7</sub> in its fibrous shape. The peaks around 3440 and 1632 cm<sup>-1</sup> of the spectrum explain the attendance of physically adsorbed water molecule. In addition, the peaks related to Dy<sub>2</sub>Ce<sub>2</sub>O<sub>7</sub> are placed at 1462, 1104 and 454 cm<sup>-1</sup>.

**Figure 3.** XRD analysis of fibrous Dy<sub>2</sub>Ce<sub>2</sub>O<sub>7</sub> NPs.

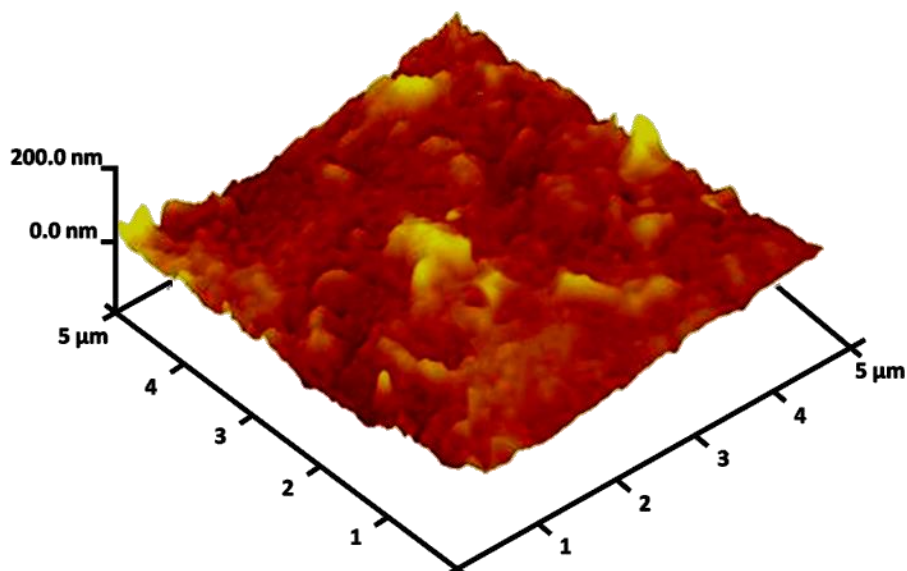


**Figure 4.** Three-dimensional of AFM images of fibrous  $\text{Dy}_2\text{Ce}_2\text{O}_7$  NPs.

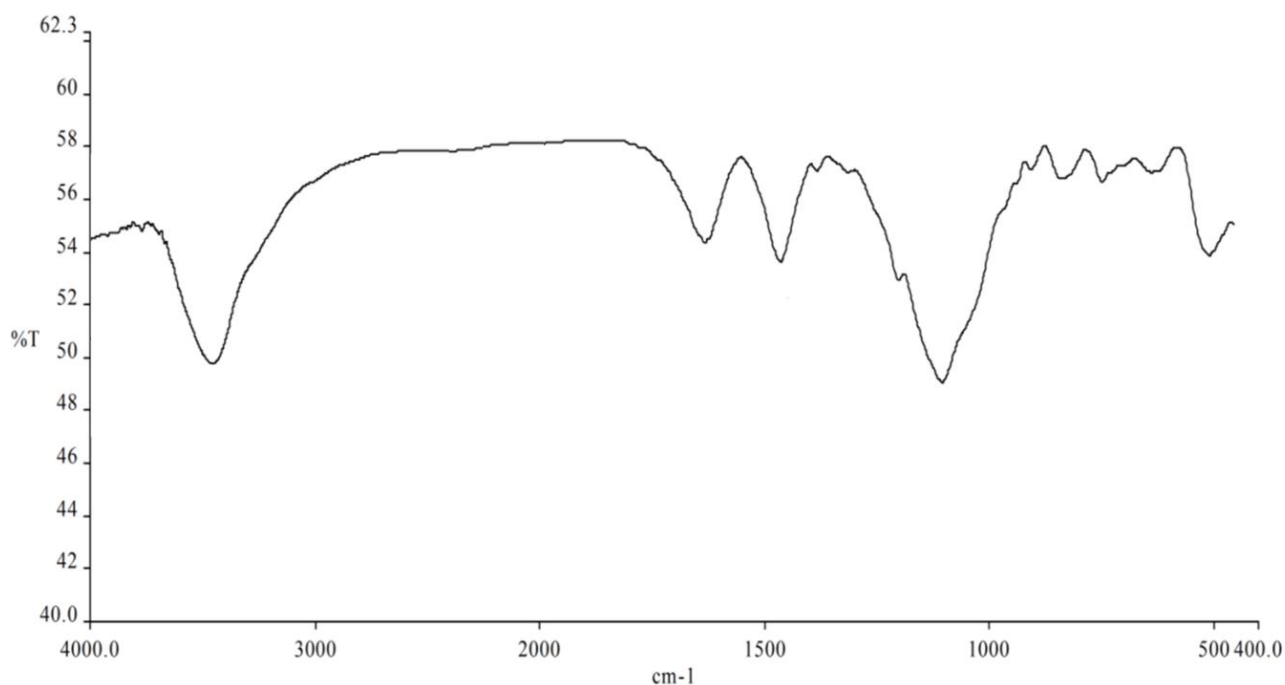


**Figure 5.** FT-IR spectrum of the produced fibrous  $\text{Dy}_2\text{Ce}_2\text{O}_7$  NPs.

In order to study the electrocatalytic activity of fibrous nano  $\text{Dy}_2\text{Ce}_2\text{O}_7$ , cyclic voltammetry (CV) and chronoamperometry of different catalysts are measured. Figure 6a shown the CV curve of different catalysts in nitrogen saturated 0.5 M  $\text{H}_2\text{SO}_4$ . The electrochemical effective area (ECSA) of the catalyst may be predicted using integral deduction of the area of hydrogen adsorption and desorption between the -0.2 and 0.1 V. The ECSA of fibrous nano  $\text{Dy}_2\text{Ce}_2\text{O}_7$  and simple nano  $\text{Dy}_2\text{Ce}_2\text{O}_7$  catalyst were 52.08 and 37.97  $\text{m}^2/\text{g}$ . Compared with the calculated results, the ECSA of fibrous nano  $\text{Dy}_2\text{Ce}_2\text{O}_7$  was larger than that of simple nano  $\text{Dy}_2\text{Ce}_2\text{O}_7$ . As shown the results in Figure

6b, a peak current was obtained by fibrous nano  $\text{Dy}_2\text{Ce}_2\text{O}_7$  yolk-shell nanoalloy (0.39 A/mg) than that of simple nano  $\text{Dy}_2\text{Ce}_2\text{O}_7$  (0.18 A/mg) at  $\sim 0.69$  V. As compared in Figure 6c, the fibrous nano  $\text{Dy}_2\text{Ce}_2\text{O}_7$  had a higher activity in term of specific area. Finally, Chronoamperometry is employed to study the electrochemical activity and stability of the catalyst. As can be seen from Figure 6d, the fibrous nano  $\text{Dy}_2\text{Ce}_2\text{O}_7$  had a much better stability compared with the simple nano  $\text{Dy}_2\text{Ce}_2\text{O}_7$ . After 5 min, the current density of the fibrous nano  $\text{Dy}_2\text{Ce}_2\text{O}_7$  is higher (0.08 A/mg) by factor of 5 times than simple nano  $\text{Dy}_2\text{Ce}_2\text{O}_7$  (0.03 A/mg), further demonstrating the better electrocatalytic durability.

The durability of fibrous nano  $\text{Dy}_2\text{Ce}_2\text{O}_7$  was further verified by cyclic voltammetry in  $\text{N}_2$ -purged 0.5 M  $\text{H}_2\text{SO}_4$ , where the electrochemically active surface area (determined from the hydrogen adsorption region) is almost kept constant with a small loss of 0.9% within 200 cycles. The improved electrocatalytic ability, strong tolerance, and better stability of fibrous nano  $\text{Dy}_2\text{Ce}_2\text{O}_7$  are attributed to two factors. (i) The dandelion-like structures contribute to a larger electrochemically active surface area and the abundant atomic steps, edges, and corner atoms in the  $\text{Dy}_2\text{Ce}_2\text{O}_7$  fibers would act as highly active sites for methanol oxidation. (ii) Better dispersion of the fibrous  $\text{Dy}_2\text{Ce}_2\text{O}_7$  nanoparticles on the enlarges the surface area and facilitates electron transport (Figure 7).

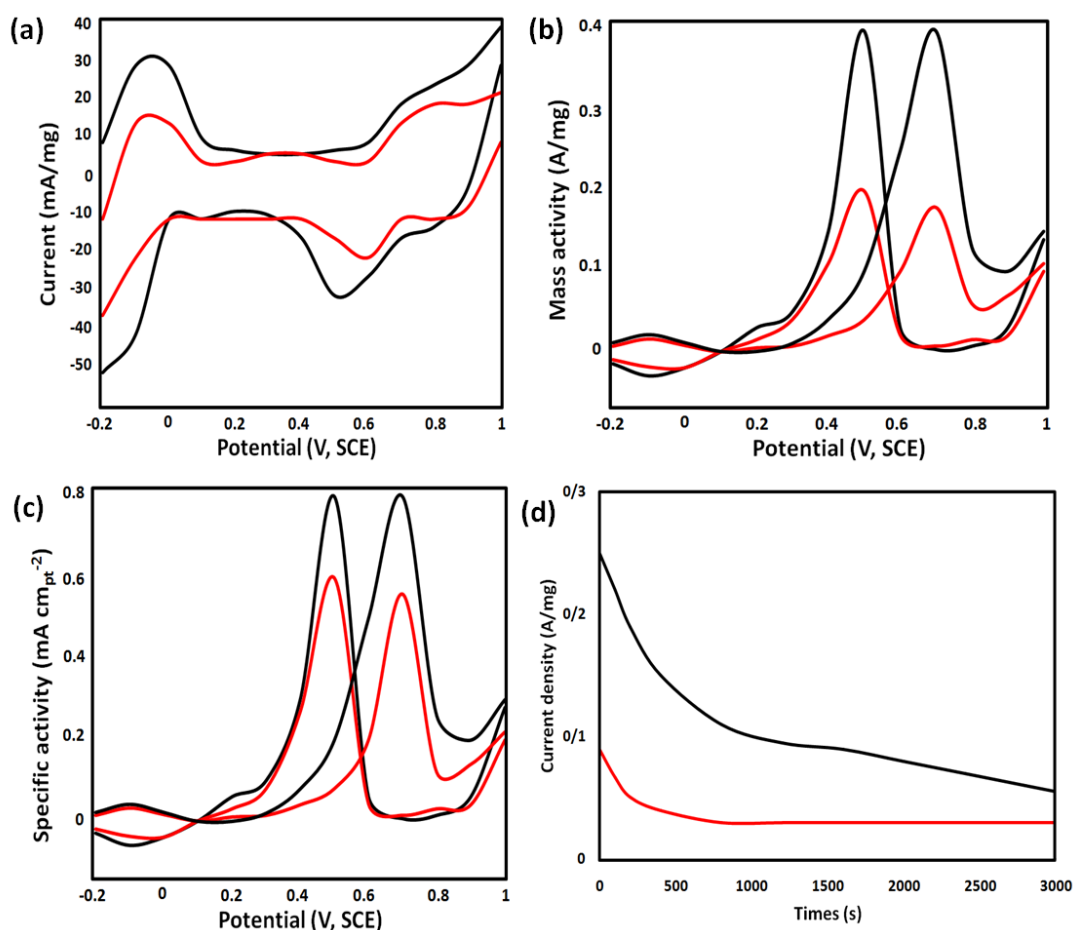


**Figure 6.** (a) CV curves of the catalysts in 0.5 mol/L  $\text{N}_2$ -saturated  $\text{H}_2\text{SO}_4$  solution; (b, c) CV curves of the catalysts in 0.5 mol/L  $\text{H}_2\text{SO}_4$  and 0.5 mol/L  $\text{CH}_3\text{OH}$  solution; (d) Chronoamperograms of different catalysts for MOR at 0.60 V for 3000 s of simple nano  $\text{Dy}_2\text{Ce}_2\text{O}_7$  (red) and the fibrous nano  $\text{Dy}_2\text{Ce}_2\text{O}_7$  structure (black).

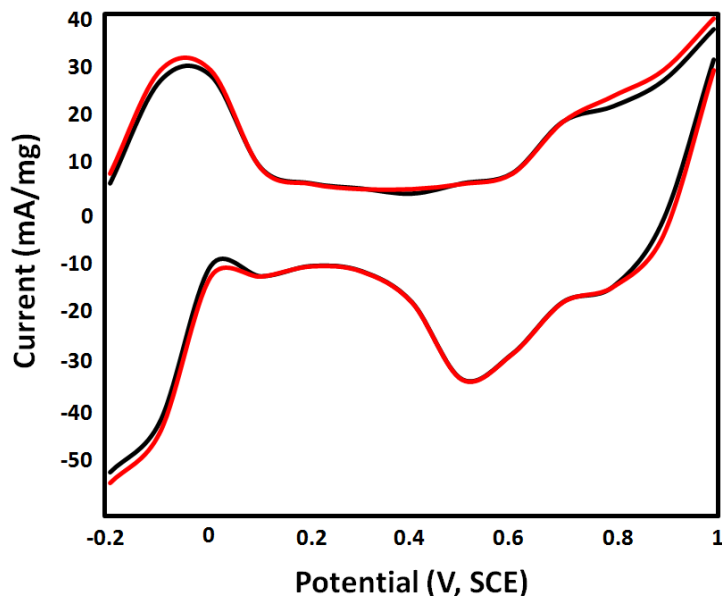


**Figure 7.** The cyclic voltammograms of the fibrous nano  $\text{Dy}_2\text{Ce}_2\text{O}_7$  electrode before and after 200 cycles in  $\text{N}_2$ -saturated 0.5 M  $\text{H}_2\text{SO}_4$ .

According to the above results of our prepared electrocatalyst, an improved performance was achieved when compared with other electrocatalysts in the literature [34-39] as shown in Table 2 as follows: The potential value of the first oxidation peak at Pd-Ni/C electrocatalyst precedes that at both Ni-Pd/Si and Ni-Pd/Si-microchannel plates, prepared by electroless plating followed by annealing at 300 °C [34] by 42 and 32 mV, respectively and that at Pd-1 wt.% MWCNTs-5 wt.% Ni electrocatalyst by 37 mV [37]. An increased current density value by 4.6 times was shown at the first oxidation peak of our Pd-Ni/C electrocatalyst, in relation to that of ethanol oxidation reaction at  $\text{Pd}_2\text{Ni}_3/\text{C}$ , prepared by solution phase-based nanocapsule method [35]. It is comparable to that obtained at  $\text{Pd}_1\text{Ni}_3/\text{C}$  electrocatalyst, prepared by impregnation method using  $\text{NaBH}_4$  as a reducing agent, during allyl alcohol oxidation [36]. As shown in Table 2, the yolk-shell structure of our catalyst was more active than other catalyst, indicating a promising application for methanol oxidation. The activity and selectivity of nano-catalyst can be manipulated by tailoring chemical and physical properties like size, shape, composition and morphology. Besides, the large space between fibers can significantly increase the accessibility of the active sites of the nanofibrous  $\text{Dy}_2\text{Ce}_2\text{O}_7$ . That is why, the nanofibrous  $\text{Dy}_2\text{Ce}_2\text{O}_7$  was more effective than other nano catalysts. As a result, nanofibrous  $\text{Dy}_2\text{Ce}_2\text{O}_7$  were used in the subsequent investigations because of its high reactivity, high selectivity and easy separation.

**Table 2.** Comparison of nano catalysts for methanol electrooxidation.

Entry	Catalyst	Preparation method	Organic substrate	Oxidation solution	<i>I</i>	Refs.
1	Ni-Pd/Si	Electroless plating followed by annealing at 300 °C	Methanol	(2 M KOH + 1 M methanol)	3.28 mA	34
2	Ni-Pd/Simicrochannel plates	Electroless plating followed by annealing at 300	Methanol	(2 M KOH + 1 M methanol)	33.93 mA	34

		°C				
3	Pd <sub>2</sub> Ni <sub>3</sub> /C	Solution phase-based nanocapsule method	Ethanol	(1 M KOH + 1 M methanol)	1.66 mA cm <sup>-2</sup>	35
4	Pd <sub>1</sub> Ni <sub>3</sub> /C	Impregnation method using NaBH <sub>4</sub>	Allyl alcohol	(0.5 M NaOH + 0.1 M allyl alcohol)	9 mA cm <sup>-2</sup>	36
5	Pd-1 wt.% MWCNTs-5 wt.% Ni	Impregnation method using NaBH <sub>4</sub>	Methanol	(1 M KOH + 1 M methanol)	341.68 mA cm <sup>-2</sup> mg <sup>-1</sup> (Pd)	37
6	Pd-Ni/MWCNTs	Impregnation method using NaBH <sub>4</sub>	Methanol	(0.5 M KOH + 1 M methanol)	482.2 mA mg <sup>-1</sup> (Pd)	38
7	Ni@Pd/MWCNTs	Core and shell method	Methanol	(0.5 M KOH + 1 M methanol)	770.7 mA mg <sup>-1</sup> (Pd)	38
8	Pd-Ni/C	Impregnation method using formic acid	Methanol	(1 M KOH + 1 M methanol)	530 mA mg <sup>-1</sup> (Pd)	39
9	Nanofibrous Dy <sub>2</sub> Ce <sub>2</sub> O <sub>7</sub>	Core and shell method	Methanol	(0.5 M H <sub>2</sub> SO <sub>4</sub> + 0.5 M methanol)	390 mA mg <sup>-1</sup> (Pd)	Our work

#### 4. CONCLUSIONS

In conclusion, fibrous Dy<sub>2</sub>Ce<sub>2</sub>O<sub>7</sub> nanoparticles was synthesized successfully by a simple method. The obtained nanoalloy was well characterized by a series of methods and used as catalyst for the electrooxidation of methanol. The fibrous nano Dy<sub>2</sub>Ce<sub>2</sub>O<sub>7</sub> showed welldefined dandelion-like structures as well as proper dissemination that exhibited enhanced electrocatalytic characteristics. Besides, fibrous nano Dy<sub>2</sub>Ce<sub>2</sub>O<sub>7</sub> denoted an improved catalytic activity and also stability for methanol oxidation. The as developed system presents a promising approach for the design of highly effective electrocatalysts for oxidation of methanol.

#### ACKNOWLEDGEMENTS

This work was supported by the Key Scientific and Technological Project of Henan Province (192102210139), the Key Scientific Research Project of Henan Province (18A180018), the Environmental Catalysis Innovative Research Team of Zhengzhou Normal University (702010), and the Student Innovative Program of Zhengzhou Normal University (DCZ2017014).

#### References

1. B. Lim, M. Jiang, P. H. C. Camargo, E. C. Cho, J. Tao, X. Lu, Y. Zhu, Y. Xia, *Science*, 324 (2009) 1302–1305.
2. L.M. Yang, Z.L. Chen, D. Cui, X. B. Luo, B. Liang, L.X. Yang, T. Liu, A. J. Wang and S. L. Luo. *Chem. Eng. J.*, 359(2019)894.
3. S. Guo, S. Dong, E. Wang, *ACS Nano*, 4 (2009) 547–555.
4. P. H. Shao, J. Y. Tian, F. Yang, X. G. Duan, S. S. Gao, W. X. Shi, X. B. Luo, F. Y. Cui, S. L. Luo and S. B. Wang, *Adv. Funct. Mater.*, 28 (2018) 1705295.
5. Q. Sun, Y. Yang, Z. Zhao, Q. Zhang, X. Zhao, G. Nie, T. Jiao and Q. Peng, *Environ. Sci: Nano*, 5 (2018) 2440.
6. H. Y. Yu, P. H. Shao, L. L. Fang, J. J. Pei, L. Ding, S. G. Pavlostathis and X. B. Luo, *Chem. Eng. J.*, 359 (2019) 176.

7. L. Shi, A. Wang, T. Zhang, B. Zhang, D. Su, H. Li, Y. Song, *J. Phys. Chem. C*, 117 (2013) 12526–12536.
8. S. F. Tang, D. L. Yuan, Y. D. Rao, M. H. Li, G. M. Shi, J. M. Gu and T. H. Zhang. *J. Hazard. Mater.*, 366 (2019) 669.
9. X. Cao, N. Wang, S. Jia, L. Guo, K. Li, *Biosens. Bioelectron.*, 39 (2013) 226–230.
10. H. Ataee-Esfahani, L. Wang, Y. Nemoto and Y. Yamauchi, *Chem. Mater.*, 22 (2010) 6310–6318.
11. R. Mezzenga, Q. R. Zhang, S. Bolisetty, Y. P. Cao, S. Handschin, J. Adamcik and Q. M. Peng, *Angew. Chem. Int. Edit.*, 2019, Doi: 10.1002/anie.201901596.
12. G. Meng, G. Ma, Q. Ma, R. Peng, X. Liu, *Solid State Ionics*, 178 (2007) 697-703.
13. Z.G. Liu, J.H. Ouyang, K.N. Sun, *Fuel Cell.*, 11 (2011) 153-157.
14. X. Cao, R. Vassen, W. Fischer, F. Tietz, W. Jungen, D. Stover, *Adv. Mater.*, 15 (2003) 1438-1442.
15. X. Y. Min, X. Wu, P. H. Shao, Z. Ren, L. Ding, X. B. Luo, *Chem. Eng. J.*, 358 (2019) 321.
16. Z. Salehi, S. Zinatloo-Ajabshir, M. Salavati-Niasari, *RSC Adv.*, 6 (2016) 26895-26901.
17. Y. Ling, J. Chen, Z. Wang, C. Xia, R. Peng, Y. Lu, *Int. J. Hydrogen Energy*, 38 (2013) 7430-7437.
18. S. Zinatloo-Ajabshir, Z. Salehi, M. Salavati-Niasari, *Journal of Alloys and Compounds*, 763 (2018) 314-321.
19. C. Wang, Y. Wang, A. Zhang, Y. Cheng, F. Chi, Z. Yu, *J. Mater. Sci.*, 48 (2013) 8133-8139.
20. C. Wang, W. Huang, Y. Wang, Y. Cheng, B. Zou, X. Fan, J. Yang, X. Cao, *Int. J. Refract. Metals Hard Mater.*, 31 (2012) 242-246.
21. F.W. Bezerra Lopes, C.P. de Souza, A.M. Vieira de Moraes, J.-P. Dallas, J.-R. Gavarri, *Hydrometallurgy*, 97 (2009) 167-172.
22. C. Sanchez-Bautista, A.J. Dos santos-García, J. Pe~na-Martínez, J. Canales-V\_azquez, *Solid State Ionics*, 181 (2010) 1665-1673.
23. E. Antolini, *J. Power Sources*, 170 (2007)1.
24. E. Antolini, E. R. Gonzalez, *Appl. Catal. B-Environ.*, 63 (2006) 137.
25. U. B. Demirci, *J. Power Sources*, 173 (2007) 11.
26. N. Kakati, J. Maiti, S. H. Lee, S. H. Jee, B. Viswanathan, Y. S. Yoon, *Chem. Rev.*, 114 (2014) 12397.
27. H. S. Liu, C. J. Song, L. Zhang, J. J. Zhang, H. J. Wang, D. P. Wilkinson, *J. Power Sources*, 155 (2006) 95.
28. N. S. Porter, H. Wu, Z. W. Quan, J. Y. Fang, *Acc. Chem. Res.*, 46 (2013) 1867.
29. Y. K. Zhou, K. Neyerlin, T. S. Olson, S. Pylypenko, J. Bult, H. N. Dinh, T. Gennett, Z. P. Shao, *Energ. Environ. Sci.*, 10 (2010) 1437.
30. X. Q. Huang, S. H. Tang, X. L. Mu, Y. Dai, G. X. Chen, Z. Y. Zhou, F. X. Ruan, Z. L. Yang, N. F. Zheng, *Nat. Nanotechnol.*, 6 (2011) 28.
31. S. J. Guo, E. K. Wang, *Acc. Chem. Res.*, 44 (2011) 491.
32. S. Sakong, A. Gross, *Acs Catal.*, 6 (2016) 5575.
33. C. Li, R. Dai, R. Qi, X. Wu, J. Ma, *Int. J. Electrochem. Sci.*, 12 (2017) 2485.
34. F. Miao, B. Tao, L. Sun, T. Liu, J. You, L. Wang, P.K. Chu, *J Power Sources*, 195 (2010) 146.
35. Z. Zhang, L. Xin, K. Sun, W. Li, *Int J Hydrogen Energy*, 36 (2011) 12686.
36. C. Jin, X. Sun, Z. Chen, R. Dong, *Mater Chem Phys.*, 135 (2012) 433.
37. R.N. Singh, A. Singh, *Int J Hydrogen Energy*, 34 (2009) 2052.
38. Y. Zhao, X. Yang, J. Tian, F. Wang, L. Zhan, *Int J Hydrogen Energy*, 35 (2010) 3249.
39. Z. Liu, X. Zhang, L. Hong, *Electrochem Commun.*, 11 (2009) 925.